



**HAL**  
open science

# Infectious Bursal Disease Virus, a Non-enveloped Virus, Possesses a Capsid-associated Peptide That Deforms and Perforates Biological Membranes

Marie Galloux, Sonia Libersou, Nelly Morellet, Serge Bouaziz, Bruno da Costa, Malika Ouldali, Jean Lepault, Bernard Delmas

## ► To cite this version:

Marie Galloux, Sonia Libersou, Nelly Morellet, Serge Bouaziz, Bruno da Costa, et al.. Infectious Bursal Disease Virus, a Non-enveloped Virus, Possesses a Capsid-associated Peptide That Deforms and Perforates Biological Membranes. *Journal of Biological Chemistry*, 2007, 282 (28), pp.20774-20784. 10.1074/jbc.M701048200 . hal-02122529

**HAL Id: hal-02122529**

**<https://hal.science/hal-02122529v1>**

Submitted on 30 May 2020

**HAL** is a multi-disciplinary open access archive for the deposit and dissemination of scientific research documents, whether they are published or not. The documents may come from teaching and research institutions in France or abroad, or from public or private research centers.

L'archive ouverte pluridisciplinaire **HAL**, est destinée au dépôt et à la diffusion de documents scientifiques de niveau recherche, publiés ou non, émanant des établissements d'enseignement et de recherche français ou étrangers, des laboratoires publics ou privés.

Copyright

# Infectious Bursal Disease Virus, a Non-enveloped Virus, Possesses a Capsid-associated Peptide That Deforms and Perforates Biological Membranes\*

Received for publication, February 5, 2007, and in revised form, May 3, 2007. Published, JBC Papers in Press, May 8, 2007, DOI 10.1074/jbc.M701048200

Marie Galloux<sup>‡1</sup>, Sonia Libersou<sup>§2</sup>, Nelly Morellet<sup>¶1</sup>, Serge Bouaziz<sup>¶1</sup>, Bruno Da Costa<sup>‡</sup>, Malika Ouldali<sup>§</sup>, Jean Lepault<sup>‡3</sup>, and Bernard Delmas<sup>‡4</sup>

From the <sup>‡</sup>Unité de Virologie et Immunologie Moléculaires, UR892, Batiment de Biotechnologies, INRA, Domaine de Vilvert, 78350 Jouy-en-Josas, the <sup>§</sup>Laboratoire de Virologie Moléculaire et Structurale, CNRS, UMR 2472, IFR 115, INRA, UMR 1157, 91198 Gif-sur-Yvette, and the <sup>¶</sup>Unité de Pharmacologie Chimique et Génétique, INSERM, U640, CNRS, UMR 8151, 75006 Paris, France

Double-stranded RNA (dsRNA) virions constitute transcriptionally competent machines that must translocate across cell membranes to function within the cytoplasm. The entry mechanism of such non-enveloped viruses is not well described. Birnaviruses are unique among dsRNA viruses because they possess a single shell competent for entry. We hereby report how infectious bursal disease virus, an avian birnavirus, can disrupt cell membranes and enter into its target cells. One of its four structural peptides, pep46 (a 46-amino acid amphiphilic peptide) deforms synthetic membranes and induces pores visualized by electron cryomicroscopy, having a diameter of less than 10 nm. Using both biological and synthetic membranes, the pore-forming domain of pep46 was identified as its N terminus moiety (pep22). The N and C termini of pep22 are shown to be accessible during membrane destabilization and pore formation. NMR studies show that pep46 inserted into micelles displays a *cis-trans* proline isomerization at position 16 that we propose to be associated to the pore formation process. Reverse genetic experiments confirm that the amphiphilicity and proline isomerization of pep46 are both essential to the viral cycle. Furthermore, we show that virus infectivity and its membrane activity (probably because of the release of pep46 from virions) are controlled differently by calcium concentration, suggesting that entry is performed in two steps, endocytosis followed by endosome permeabilization. Our findings reveal a possible entry pathway of infectious bursal disease virus: in endosomes containing viruses, the lowering of the calcium concentration promotes the release of pep46 that induces the formation of pores in the endosomal membrane.

Biological membranes represent a physical barrier that isolates cellular components from the external environment. Exchanges between cells and their surroundings are brought about by structural changes of the lipid bilayer that lead either to fusion events (vesicular trafficking) or to the formation of pores (exchange through channels). Membrane-enveloped and non-enveloped viruses represent a paradigm for the study of membrane deformations (1). Enveloped viruses carry membrane-anchored glycoproteins that mediate fusion between viral and cellular membranes. The considerable number of studies carried out on viral glycoproteins, in particular the large number of x-ray crystal structure determinations (2–5) have shed light on the membrane fusion mechanism. In contrast, the entry pathway of non-enveloped viruses is not as well understood. For positive-strand RNA (+sRNA) viruses such as poliovirus, binding of the virus to its receptor results in large capsid rearrangements. The hydrophobic N terminus of the VP1 protein moves to the particle surface while the myristoylated internal protein VP4 inserts into the target membrane (6, 7). Nodaviruses, others +sRNA viruses, have a unique capsid protein (8) associated to a peptide, the  $\gamma$  peptide (44 residues). Both capsid protein and peptide result from the self-cleavage of a capsid protein precursor. The  $\gamma$  peptide has the capacity to permeabilize biological membranes allowing genome translocation through the membrane (9, 10). The recent determination of the atomic structure of the  $\gamma$  peptide membrane-active domain demonstrates similarities with the fusion peptides of glycoproteins of enveloped viruses: both are formed by a kinked helix (11). The  $\gamma$  peptide is located inside the capsid and is brought toward the membrane during entry. For these viruses, all these rearrangements are believed to result in the formation of a narrow channel that allows the genomic RNA to reach the cytoplasm. In contrast to +sRNA viruses, dsRNA viruses have to maintain their genome hidden from the cellular defense mechanisms at all steps of the viral cycle. Consequently, a large object, the capsid-protected genome, needs to cross the cell membrane. Most dsRNA viruses possess several concentric shells. During entry, the external capsid layer is generally lost and its constitutive proteins, or their cleavage products, are thought to induce a local destabilization of the cellular membrane allowing virus translocation (12). Recently, it has been shown that mammalian reovirus produce a myristoylated peptide ( $\mu$ 1N) that can induce size-selective pores in membranes

\* This work was supported by a grant of the ACI "Microbiologie" from the French MRT, by the EU COST action 892, and the Agence Nationale de la Recherche "Projets blancs" programs. The costs of publication of this article were defrayed in part by the payment of page charges. This article must therefore be hereby marked "advertisement" in accordance with 18 U.S.C. Section 1734 solely to indicate this fact.

The atomic coordinates and structure factors (code 2IMU) have been deposited in the Protein Data Bank, Research Collaboratory for Structural Bioinformatics, Rutgers University, New Brunswick, NJ (<http://www.rcsb.org/>).

<sup>1</sup> Funded by an INRA/Région Ile-de-France fellowship.

<sup>2</sup> Supported by an INRA fellowship.

<sup>3</sup> To whom correspondence may be addressed. Tel.: 33-1-6982-3855; E-mail: jean.lepault@vms.cnrs-gif.fr.

<sup>4</sup> To whom correspondence may be addressed. Tel.: 33-1-3465-2627; Fax: 33-1-3465-2621; E-mail: bernard.delmas@jouy.inra.fr.

(13). The release of this peptide associated to pore formation (13) and structural rearrangements of the remaining domain of  $\mu 1$  ( $\mu 1$  C) (14) are thought to lead to virus entry into the cell. Birnaviruses only possess a single-layered capsid (15) that is assumed to be competent for both virus translocation and genome replication-transcription. For all dsRNA<sup>5</sup> viruses, the mechanisms of membrane destabilization associated to entry remain hypothetical. Totiviruses, another group of dsRNA viruses that lack additional shells constitute a special case because they are not able to enter into a cell and are therefore only transmitted during cell division.

The capsid of birnaviruses is formed by 260 VP2 protein trimers (15, 16) which obey  $T = 13$  laevo icosahedral symmetry (17, 18). VP3, the second major viral protein, binds the RNA-dependent RNA polymerase VP1 and the genomic dsRNA (19, 20). Birnaviruses present characteristic peptides associated to the virus particle (21). Four peptides (pep46, pep7a, pep7b, and pep11) being 46, 7, 7, or 11 amino acids in length, respectively, are found in the case of infectious bursal disease virus (IBDV) (22). These peptides are generated through the processing of the viral polyprotein pVP2-VP4-VP3 (Fig. 1). VP4 is a protease that cleaves its own N and C termini, thus releasing pVP2 and VP3 within the infected cell (23). Subsequent serial cleavages at the C terminus of pVP2 yield the mature VP2 capsid protein and the four peptides.

In this study, we show that pep46 deforms biological membranes, leading to the formation of pores. We determined by NMR the atomic structure of this peptide. The membrane-active domain is formed by two kinked  $\alpha$ -helices linked by a proline displaying *cis-trans* isomerization that controls peptide hydrophobicity. These results combined with reverse genetic studies permit the proposition of a general model describing the cell entry pathway of a non-enveloped virus.

## EXPERIMENTAL PROCEDURES

**Peptide Synthesis**—The peptides were obtained by automated solid-phase synthesis using the 9-fluorenylmethoxy carbonyl strategy and purified by reversed-phase high-performance liquid chromatography using standard procedures. The peptides were analyzed by mass spectrometry and confirmed to have purity higher than 98%.

**Peptide Activity**—The hepatocarcinoma epithelial chicken LMH cell line was grown in RPMI medium supplemented with 10% fetal calf serum, 2 mM glutamine, and 1 mM sodium pyruvate. The activity of the peptides was determined by studying their effects on live cells. After incubation at 37 °C, LDH release was measured using the cytotox 96 nonradioactive kit (Promega), as described by the manufacturer. The percentage of LDH release was determined taking in account the OD values found on untreated and Triton X-100-treated cells. All experiments were carried out five times on duplicated samples; all measurements gave similar results. Liposomes containing carboxyfluorescein (CF) were prepared as described by Nandi *et al.*

(24). The release of CF after addition of peptides or virus was monitored by the increase of fluorescence at 520 nm, using a 492-nm excitation band in a thermostatted Perkin-Elmer LS50B spectrofluorimeter. The value for 100% release was obtained by addition of Triton X-100 at the end of the reaction. All fluorescent experiments were carried out at least three times and gave similar results.

**Electron Cryomicroscopy**—Microscopy was performed as previously described (25). A drop of the studied sample was adsorbed to air glow-discharged holey carbon films. The excess of liquid was removed and the grid frozen in liquid nitrogen cooled ethane. The grid was transferred into a Gatan 6226 cryo-holder and observed with a Philips CM12 electron microscope operated at 80 kV. The micrographs were recorded at a magnification of 35,000 under standard low dose exposition conditions.

**Sample Preparation and NMR Spectroscopy**—Pep46 was dissolved at pH 3.5 in an aqueous 40 mM dodecylphosphocholin (DPC) solution at a final concentration of 1 mM. Two-dimensional phase-sensitive <sup>1</sup>H Clean-TOCSY with 70 ms spin lock, and 100 ms and 200 ms mixing times NOESY experiments (26) were recorded at 313 K and 333 K on an AVANCE Bruker spectrometer operating at 600.14 MHz without sample spinning with 2K real points in *t*<sub>2</sub>, with a spectral width of 6000 Hz and 512 *t*<sub>1</sub>-increments. Pulsed-field gradients (27) were used for water suppression. The data were processed using XWIN-NMR software (Bruker). A  $\pi/6$  phase-shifted sine bell window function was applied prior to Fourier transformation in both dimensions (*t*<sub>1</sub> and *t*<sub>2</sub>). The temperature was externally controlled using a special temperature control system (BCU 05 Bruker).

**NMR Structure Determination**—NOE cross-peak volumes measured on NOESY spectrum (NOESY, 200 ms mixing time, 333 K) were converted into distances, semiquantitatively, by counting contour levels. Using the Tyr-2,6H geminal, and Asp-H $\beta$  protons as calibration peak, NOE signals were classified into 5 categories with upper distance limits ranging from 2.5 to 5 Å. Pseudo-atom corrections were added when necessary. Calculations were performed using the standard procedures in X-PLOR version 3.84 (28, 29). Quality of structures was evaluated with PROCHECK (30).

**Virus Rescue Experiments**—To generate infectious IBDV mutants from cDNA clones, a previously described strategy was used (22). Cells at 90% confluence in P12 wells were infected with the vaccinia virus MVA-T7 at a multiplicity of infection of 1. After a 1-h adsorption, the cells were rinsed with the RPMI medium. In the mean time, pT7-A-HDR derivatives and pT7-B-HDR plasmids allowing the transcription of genome segments A and B, respectively, were mixed (0.5  $\mu$ g of each plasmid) with 3.5  $\mu$ l of Lipofectamine 2000 (Invitrogen) in 350  $\mu$ l of OptiMEM and were kept at room temperature for 30 min. The cells were again rinsed in OptiMEM and incubated with the DNA-Lipofectamine 2000 mixture at 37 °C for 5 h. Next, 1.5 ml of complemented RPMI medium was added to each well. Recombinant mutant viruses were recovered 48-h post-transfection after filtration through a 0.22- $\mu$ m-pore-size filter. At least three independent transfection experiments were carried out to analyze each pT7-A-HDR derivative. The viruses were amplified

<sup>5</sup> The abbreviations used are: dsRNA, double-stranded RNA; LDH, lactate dehydrogenase; CF, carboxyfluorescein; IBDV, infectious bursal disease virus; DPC, dodecylphosphocholin; VLP, virus-like particles; r.m.s.d., root mean-squared deviation.

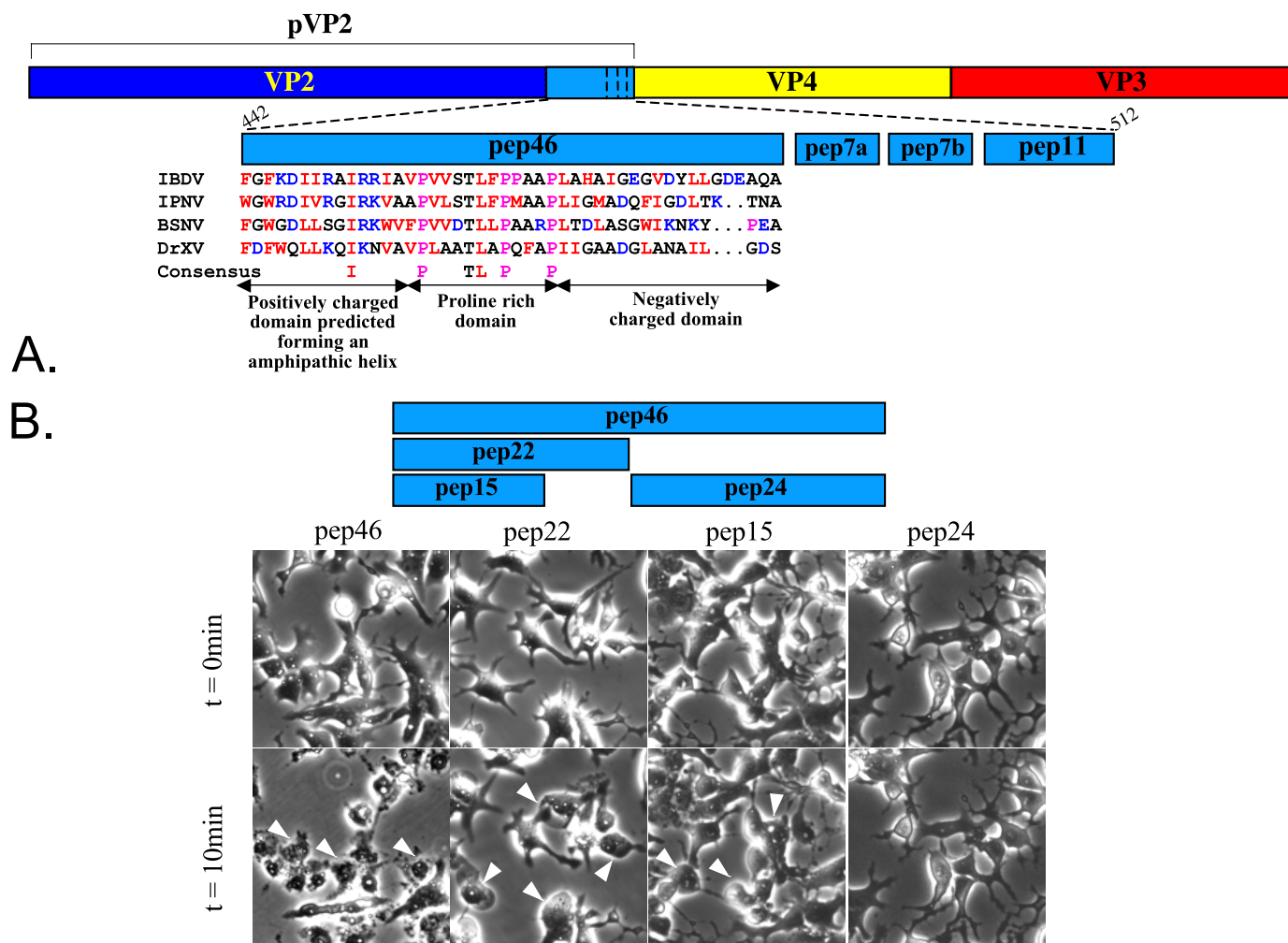


**FIGURE 1. Schematic representation of the IBDV polyprotein processing and effects of pep46 and derivatives on cell morphology.** A, IBDV polyprotein and the four structural peptides pep46, pep7a, pep7b, and pep11 derived from the C-terminal domain of pVP2, are represented. Numbering refers to the amino acid position in the polyprotein. Hydrophobic residues are red, and charged residues are blue. Strictly conserved residues are indicated in the consensus line. The main characteristics of the pep46 domains are indicated. B, effect of pep46 and derivatives on the morphology of LMH cells. After 10 min, drastic effects on the morphology and the size of the cells are observed with pep46 and pep22 and to a lesser extent with pep15. Pep24 has no effect on cells. Major morphological effects are indicated by white arrowheads.

on LSCC-BK3 cells. IBDV-infected LSCC-BK3 cells were analyzed 3 or 5 days postinfection. Briefly, the cells were fixed with 2.5% PFA in phosphate-buffered saline for 30 min at room temperature and permeabilized by incubation for 10 min in 0.1% Triton X-100. Fixed cells were incubated with a 1:250 dilution of an anti-VP3 monoclonal antibody. Next, the cells were rinsed and incubated with an anti-immunoglobulin mouse fluorescein isothiocyanate conjugate in phosphate-buffered saline-0.05% Tween. The cells were rinsed three times and subjected to FACS-calibur (Becton Dickinson) analysis using the Cell Quest Pro software.

**VLP-GFP Cell Binding Assay**—Fluorescent VLP were produced as described by Chevalier *et al.* (31). The VLP were incubated on permissive and non-permissive cells at 4 °C for 30 min in the presence and absence of calcium. The cells were rinsed twice with OptiMEM (Invitrogen) containing the adequate concentration of calcium and analyzed with the FACS-calibur.

## RESULTS AND DISCUSSION

**The Membrane-active Domain of pep46**—Fig. 1A shows the schematic representation of the IBDV polyprotein mat-

uration process. A sequence alignment between different birnavirus pep46 homologues reveals only six conserved residues, three of them proline. All sequences display identical clusters of similar amino acids allowing the definition of three domains: the central hydrophobic domain containing most of the conserved residues (three prolines at positions 16, 23, and 27, a threonine at position 20 and the following leucine) and the two flanking domains mainly constituted by both hydrophobic and charged residues. Whereas the N-terminal domain is positively charged, the C-terminal is somewhat negatively charged. The N-terminal domain is predicted as forming an amphipathic  $\alpha$ -helix with positively charged residues on one side of the helix and hydrophobic residues on the other side (22). As far as the positions of charged and hydrophobic residues are concerned, the sequence similarity between pep46 of different IBDV strains (data not shown) and different birnaviruses (Fig. 1A) is higher in the N-terminal than in the C-terminal domain, suggesting a critical role of this  $\alpha$ -helix in the viral cycle. The overall hydrophobicity of pep46 strongly suggests potential

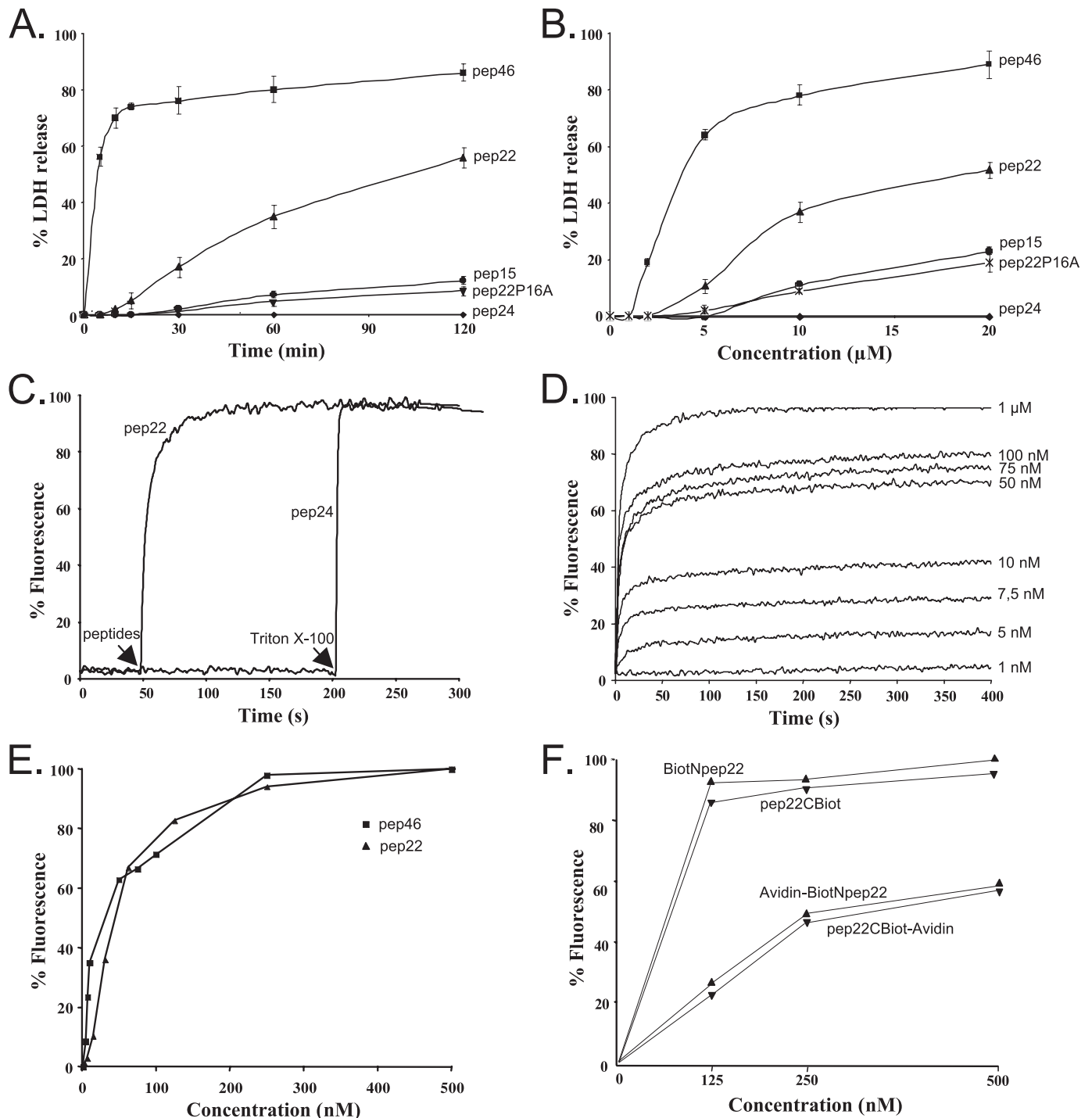
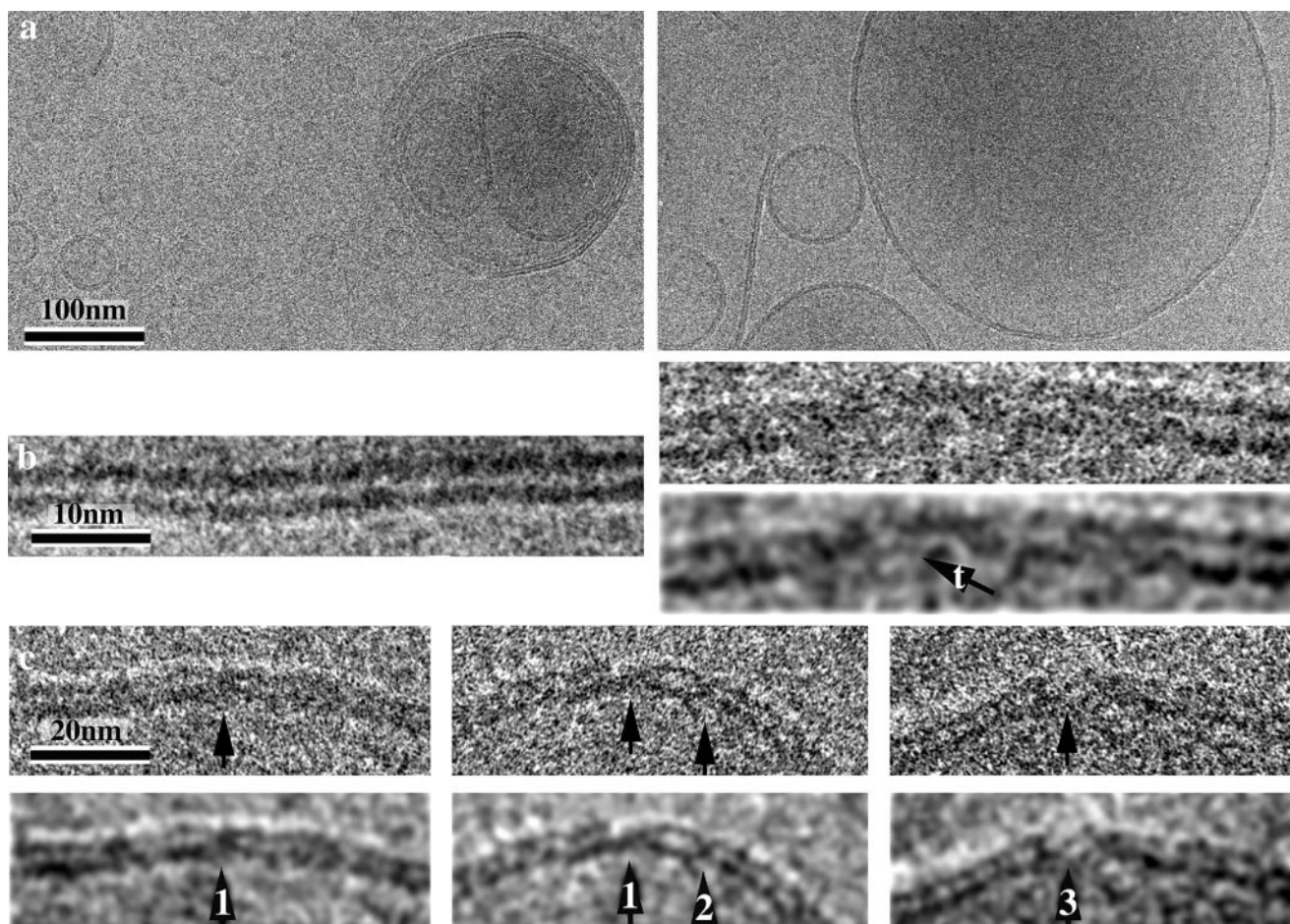


FIGURE 2. Membrane permeabilization activity of pep46 and derivatives. *A* and *B* show the peptide activity on cells quantified by LDH release and expressed as a percentage of the total cellular LDH. *A*, effect of time on LDH release. Peptides were incubated with cells at a concentration of 10 µM. The amino acid sequence of pep22P16A is identical to the one of pep22 except proline in position 16 that is substituted by an alanine. No release was observed with pep24. *B*, effect of concentration on LDH release. The activities of pep15 and pep22P16A display the same concentration dependence. Again, no activity could be observed with pep24. *C* and *D* show the release of the fluorescent probe from synthetic liposomes. The peptide activity was quantified by the fluorescent probe leakage and expressed as a percentage of the total unquenched fluorescence (when liposomes were treated with Triton X-100). In *A* and *B*, results are mean ± S.D. of five distinct experiments. *C*, activities of pep22 and pep24 at a concentration of 1 µM were compared. Triton X-100 indicates the time at which Triton X-100 has been added to the samples to validate the quality of the liposomes containing the fluorescent probe. Again, no activity of pep24 was detected. *D*, effect of peptide concentration and time. The activity of pep46 was measured and found concentration dependent in the nanomolar to micromolar range. *E*, comparison of the effects of pep46 and pep22 on liposomes. *F*, effect of avidin binding at the N and C terminus of pep22.

interactions of this peptide with membranes. Fig. 1*B* shows that cells incubated with pep46 undergo spectacular morphological modifications characterized by significant shrinkage and cytoplasm vacuolization. Video light micros-

copy shows that pep46-treated cells first swell and then undergo important membrane deformations that are associated to massive losses of cellular material (not shown). All these changes result in round ghost cells that have lost their

## A Viral Peptide Deforms and Perforates Membrane



**FIGURE 3. Visualization by cryomicroscopy of the structural effects induced by pep22.** *a*, panels show the liposomes in the absence (*left*) and the presence (*right*) of pep22. In both cases, liposomes having various diameters are observed. In general, they are unilamellar. The bilayered structure of the membrane is clearly visible. *b*, when the membranes are observed at higher magnification, significant differences are observed in the presence of pep22. While the position of the polar heads of the lipids gives rise to parallel lines over long distances when pep22 is absent (*left*), the positions of the polar heads differ in the presence of pep22 (*right*). For this last case, the raw micrograph is presented (*upper panel*) as well as a filtered image for the low (1/100 nm) and high (1/2 nm) spatial frequencies (*lower panel*). In this last case, the thickness of the membrane seems to vary and parallel lines alternate with the fuzzy area. The *arrows* indicate a thinner membrane area (*t*). *c*, fusion events between the external and internal leaflets are observed giving rise to an aqueous channel or pore. The membrane deformations (*arrow 1*) and the pores (*2* and *3*) are better observed on images that have been filtered (*lower panel*). The diameter of the pores are less than 10 nm.

initial morphology (Fig. 1*B*). As already shown for mammalian reoviruses (Agosto *et al.*, 13), these observations can be interpreted as arising from partial permeabilization of the cellular membrane that leads to the establishment of a high osmotic pressure, resulting in severe cell damage. To identify the membrane-active domain of pep46, several peptides derived from its primary sequence, were synthesized and their effects analyzed on cells. Peptides made of the first 15 (pep15), of the 22 N-terminal amino acids (pep22) and of the last 24 C-terminal residues (pep24) were synthesized (Fig. 1*B*). Although attenuated, the effects of both pep22 and pep15 were similar to that of pep46 with a rounding of the cells and a loss of cellular material. While pep22 was found to be more efficient than pep15, pep24 had no effect on cells. All these observations demonstrate that pep46 and in particular its N-terminal moiety, pep22, destabilize cell membranes.

**The Permeabilizing Activity of pep46**—The permeabilizing activity of pep46 and its shorter derivatives, pep22, pep15, and pep24 was quantified by measuring the release of a cytoplas-

mic enzyme (LDH) induced by each peptide. Although the results are only illustrated for an IBDV-permissive cell line (LMH cells; Fig. 2), similar data were obtained for both permissive and non-permissive cells. The effects of the peptides were analyzed for time (Fig. 2*A*) and concentration (Fig. 2*B*) dependence. Fig. 2*A* shows that the peptides permeabilize membranes with characteristic kinetic constants and lag periods. While a lag period cannot be evaluated in the case of pep46, its existence is clearly visible for pep22 and pep15. Pep15 displays a longer lag period than pep22. The existence of a lag period indicates that the membrane permeabilization is a multi-step event. No activity could be detected for pep24. Fig. 2*B* shows that all peptides are characterized by a critical concentration below which the peptides have no effect on the LDH release. The critical concentration increases evenly following the order of the series: pep46, pep22, and pep15. No effect could be detected for pep24 up to a concentration of 20  $\mu\text{M}$ . All these experiments demonstrate that pep46 and particularly its N-terminal moiety permeabilize cell membranes. To assess the efficiency of pep46, we compared its

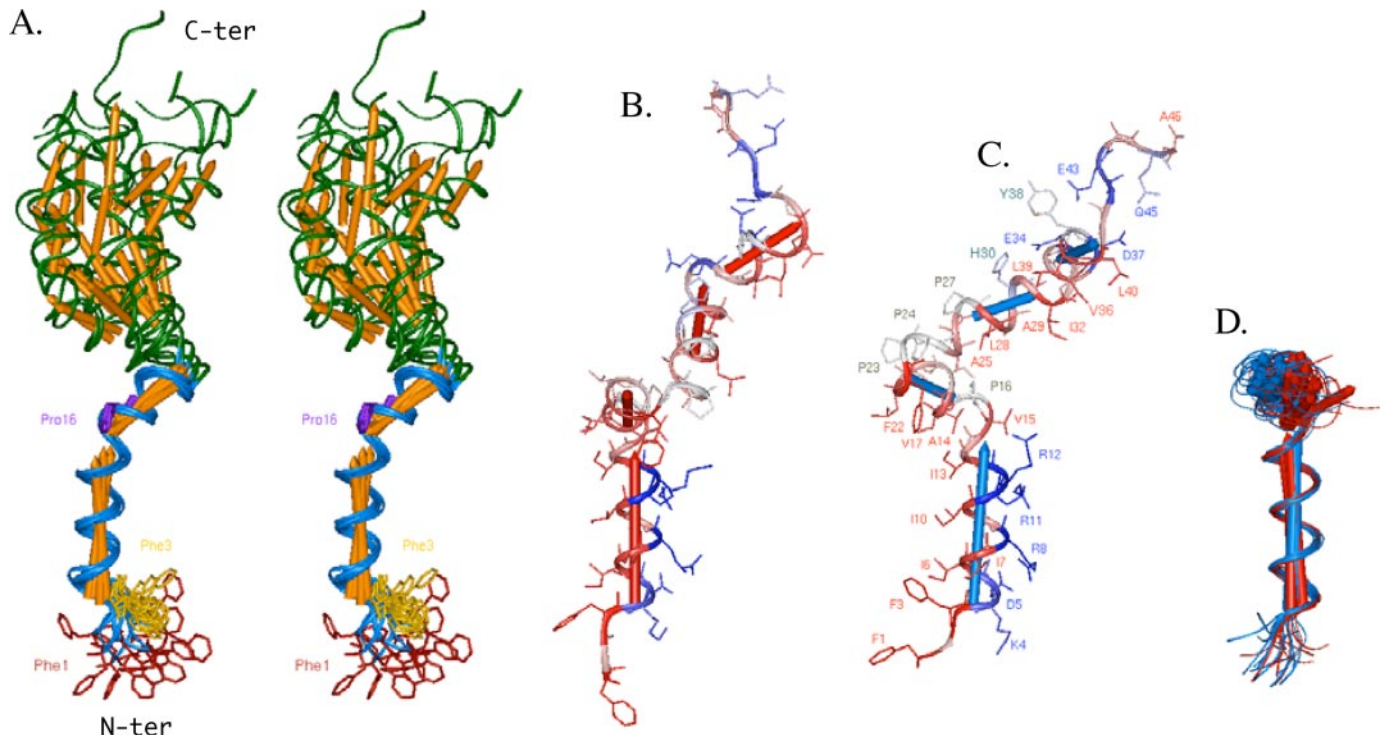


FIGURE 4. **NMR structure of pep46 in DPC micelles.** *A*, stereoview of the twelve pep46 accepted refined structures with the peptide bonds of Pro<sup>16,23,24,27</sup> in the *trans* conformation. The superposition is performed on the (3–22) backbone atoms of pep46. The ribbons corresponding to the (1–22) and (23–46) domains are respectively colored in blue and dark green. The four  $\alpha$ -helices are represented as orange cylinders. Proline 16 is colored in purple. The hydrophobic and aromatic residues, Phe<sup>1</sup> (red) and Phe<sup>3</sup> (yellow) of pep46, show a very great flexibility, which could be important for the membrane interaction. *B*, structure of one of the pep46 structures with all the prolines in the *trans* conformation, showing the distribution of the hydrophobic and hydrophilic residues along the four helices (red cylinders). *C*, influence of the *cis-trans* isomerism of the peptide bond between Val<sup>15</sup> and Pro<sup>16</sup> on the relative orientation of the (3–15) and (16–22) helices (blue cylinders). The structure should be compared with that represented in *B*. The superposition between the two structures was done on the (3–15) backbone atoms. The second helix (16–22), entirely hydrophobic, tends to be directed to the same side as the hydrophobic face of the first amphipathic helix, and, more specifically toward the residues Phe<sup>1</sup> and Phe<sup>3</sup> located at the N-extremity of Pep46, when Pro<sup>16</sup> adopts a *cis* conformation. *D*, superposition on the (3–15) backbone atoms of the best pep46 structures calculated with the proline 16 in *trans* (red cylinders) and *cis* (blue cylinders) conformation, showing the orientation distribution of the (16–22) helix toward the (3–15) helix.

activity to the one of the membrane-active domain ( $\gamma$ 1) of the nodavirus  $\gamma$  peptide. We found that  $\gamma$ 1 is 10–20-fold less efficient than pep22. While it can be seen on Fig. 2*B* that the critical concentration of pep22 is about  $3\mu\text{M}$ , the one of  $\gamma$ 1 peptide is equal to 30–50  $\mu\text{M}$  (data not shown).

The membrane permeabilization induced by pep46 could depend on a perturbation of the metabolism that controls cellular entry processes such as endocytosis. To test this hypothesis, we analyzed the influence of a metabolic inhibitor. The depletion of the cellular ATP pool did not influence the activity of pep46 and its shorter derivatives (not shown). Therefore, pep46 and in particular, its N-terminal moiety (pep22), display a membrane activity that is energy-independent. All these features were observed on permissive and non-permissive cells, demonstrating that pep46 or derivatives interact with the lipid bilayer, resulting in the formation of a pore, even in the absence of a specific receptor.

To further characterize the pore formation mechanism, we studied the activity of these peptides on synthetic membranes. The peptides were incubated with liposomes containing a fluorescent probe, which due to quenching effects has a fluorescence signal strongly depending upon concentration. The release of the probe from the liposomes leads to a lowering of the probe concentration and thus to an increase of the fluorescence signal. With pep22, at a concentration of  $1\mu\text{M}$ , the release

of the probe from liposomes is achieved within a few seconds (Fig. 2*C*). Up to a concentration of 2 mM, the release is independent of the presence of calcium or a chelating molecule (EDTA, data not shown). With this assay as with others, pep24 is found to be inactive on membranes. Fig. 2, *D* and *E* panels illustrate the results obtained with both pep46 and pep22. The release of the probe from the liposomes has kinetic characteristics similar to those previously described on cultured cells: the existence of a critical concentration and short lag period particularly visible at low concentrations. Because of the membrane composition and cell organization, the fluorescence assay on liposomes allows the detection of pores at concentrations that are three orders of magnitude lower than the LDH release assay.

**Polarity in the Interaction of pep22 with Membranes**—To analyze the importance of the N and C termini of pep22 in membrane destabilization, a reporter protein, fluorescent streptavidin, was attached either at its N or C terminus. The labeled pep22 were added to liposomes containing a fluorescent probe. Fig. 2*F* shows that the binding of avidin to either the N or the C termini of pep22 inhibits, but does not block the release of the probe from the liposomes treated with the peptide. These results demonstrate that the addition of an exogenous charged polypeptide at both termini does not prevent the formation of pores in synthetic membranes.

**TABLE 1**  
NMR restraints and structural statistics

NMR derived distance restraints		
Total	461	
Intraresidue	206	
Sequential ( $ i-j  = 1$ )	134	
Medium-range ( $1 <  i-j  \leq 4$ )	116	
Long-range ( $ i-j  > 5$ )	5	
Distance violations		
>0.2	0	
R.m.s.d. (Å) from experimental		
Distance restraints	(479*) $0.020 \pm 0.003$	
R.m.s.d. from idealized geometry		
Bonds (Å)	(715) $0.0041 \pm 0.0001$	
Angles (deg)	(1299) $0.69 \pm 0.02$	
Improper angles (deg)	(45) $0.47 \pm 0.02$	
Xplor potential energies		
$E_{\text{NOE}}$ (kcal/mol)	$10.71 \pm 3.1$	
$E_{\text{vdw}}$ (kcal/mol)	$-167.8 \pm 12.1$	
$E_{\text{total}}$ (kcal/mol)	$-1665.3 \pm 24.2$	
Ramachandran analysis of residues		
Favored region (%)	86.3	
Additional allowed regions (%)	12.8	
Generously allowed regions (%)	0.4	
Disallowed regions (%)	0.4	
Pairwise rms deviation (Å)		
	Backbone atoms	Heavy atoms
(3–15)	$0.41 \pm 0.18$	$1.49 \pm 0.44$
(17–22)	$0.36 \pm 0.17$	$0.92 \pm 0.30$
(3–22)	$0.77 \pm 0.33$	$1.63 \pm 0.48$
(18–27)	$0.87 \pm 0.39$	$1.14 \pm 0.40$
(27–33)	$0.48 \pm 0.18$	$1.09 \pm 0.36$
(35–40)	$0.32 \pm 0.14$	$1.17 \pm 0.42$

Both peptide termini are thus accessible during the pore formation process and remain in the vicinity of the polar heads of the membrane.

**Visualization of the Pores by Electron Cryomicroscopy**—The deformations of synthetic membranes induced by pep46 and shorter derivatives were analyzed by electron cryomicroscopy. Fig. 3a shows liposomes visualized in the absence (*left*) and presence (*right*) of pep22. Pep46 has similar effects on liposomes than pep22. At low magnification, both samples appear similar. Although multi-lamellar vesicles are visible, most of the liposomes are uni-lamellar and characterized by heterogeneous diameter values. Polar head and aliphatic chain domains of the lipid constituting the liposome bilayer are easily discerned. At higher magnification, a significant effect of pep22 on liposomes is observed (Fig. 3b). Whereas in the absence of pep22, the polar heads constituting the liposome bilayers form lines that are parallel over long distances (*left*), in the presence of pep22, the lines are parallel over much smaller distances (*right*). In fact, in this latter case, the bilayer thickness varies giving rise to areas characterized by the presence of parallel lines that rapidly alternate with fuzzy lines. In accordance with this observation, the contrast of the membrane is lowered when pep22 is added to the liposomes. The fuzzy domains often show fusion of the external and internal leaflets of the bilayers (Fig. 3c) demonstrating the formation of an aqueous channel within the membrane that will be defined as a pore. The diameter of the pore is not constant; while it is smaller than the picture resolution (about 2 nm) in the *left* and *middle panels*, it is larger in the *right panel*, but the diameter of the pores were always found less than 10 nm. In all cases, the diameter of the pore is smaller than the diameter of the IBDV virion (60–70 nm).

No significant effect of pep24 on liposomes could be observed (not shown).

**NMR Structure of pep46 in Dodecylphosphocholine (DPC) Micelles**—To further study the ability of the peptides to form pores, the structure of pep46 in a detergent mimicking the lipid bilayer environment was determined by NMR spectroscopy. Medium range NOE demonstrate that in DPC, pep46 is organized as four  $\alpha$ -helices (amino acids 3 to 15 or (3–15)), (16–22), (27–33), and (35–40) (Fig. 4, A and B; Table 1). The proline-rich domain is thus constituted by the second  $\alpha$ -helix and the following loop. Long range NOE are found between Val<sup>18</sup> and Ala<sup>25</sup> and between Ser<sup>19</sup> and Ala<sup>26</sup> showing that this domain has a tertiary folding mainly maintained by hydrophobic interactions. Importantly, characteristic sequential NOE cross-peaks reveal that Pro<sup>16</sup> and Pro<sup>23</sup> are present in both *cis* and *trans* conformations. The doubling of the resonances of Ala<sup>14</sup>, Val<sup>15</sup>, Val<sup>17</sup>, Val<sup>18</sup>, Phe<sup>22</sup>, Ala<sup>25</sup>, Ala<sup>26</sup>, His<sup>30</sup> confirms the *cis/trans* isomerization of several peptidyl-prolyl bonds. The all-*trans* conformation of pep46 was initially calculated. The N-terminal moiety displays two  $\alpha$ -helices with well-defined orientations (Fig. 4A). This structure is similar to that of the nodavirus membrane-active domain of the  $\gamma$  peptide (11). In the case of IBDV, the elbow between the two helices is generated by the presence of a proline, Pro<sup>16</sup>. The C-terminal moiety also shows two helices but having various possible orientations. Fig. 4B shows the best structure calculated for pep46. The (3–15) helix displays the characteristic features of an amphipathic  $\alpha$ -helix with the polar amino acids (Lys<sup>4</sup>, Asp<sup>5</sup>, Arg<sup>8</sup>, Arg<sup>11</sup>, and Arg<sup>12</sup>) located at one side and the hydrophobic residues (Ile<sup>6</sup>, Ile<sup>7</sup>, Ile<sup>10</sup>, and Ile<sup>13</sup>) at the opposite side. The second helix (16–22) is mainly hydrophobic and is followed by a proline-rich loop (23–27). The C-terminal moiety is constituted by two short helices (27–33) and (35–40) is separated by a flexible segment containing two glycines, Gly<sup>33</sup> and Gly<sup>35</sup>. The (35–40) helix is also amphipathic, with the hydrophilic face constituted by the amino acid side chain of Glu<sup>34</sup>, Asp<sup>37</sup>, and Tyr<sup>38</sup>, and the hydrophobic one by the side chains of Val<sup>36</sup>, Leu<sup>39</sup>, and Leu<sup>40</sup>.

To emphasize the influence of the Pro<sup>16</sup> *cis* conformation on pep46 structure, we generated a model by simulated annealing. Fig. 4, C and D show that the *cis*-isomerization of Pro<sup>16</sup> induces a reorientation of the second helix. In fact, the hydrophobic side of the second helix (16–22) turns toward the hydrophobic side of the first helix (3–15) and the hydrophobic residues Phe<sup>1</sup> and Phe<sup>3</sup>. The *trans* to *cis* isomerization of Pro<sup>16</sup> results in the spatial clustering of hydrophobic residues of pep46 and thus may play an important role in membrane permeabilization.

To confirm the importance of Pro<sup>16</sup> in the membrane destabilization process, a peptide corresponding to the 22 first N-terminal residues of pep46 with the Pro<sup>16</sup> substituted to an alanine (named pep22P16A) was synthesized and assayed for its ability to form pores in liposomes. Fig. 2, A and B shows that this peptide has a low permeabilization activity in comparison to pep22. It has in fact an activity similar to that of the 15 amino acid long peptide, pep15. These data show that the first 15 N-terminal amino acids are

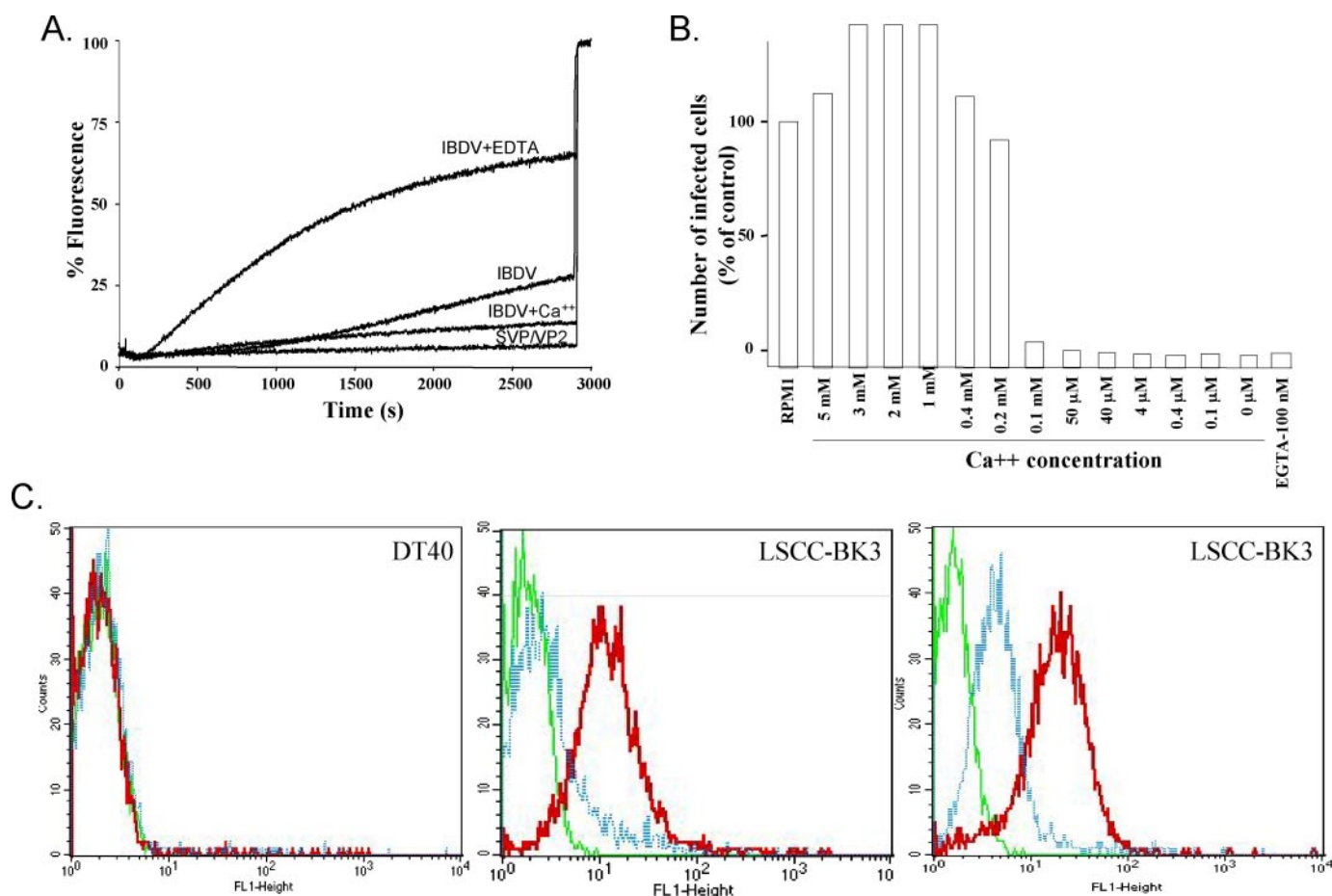


**FIGURE 5. Effect of calcium on pore formation and virus infection.** *A*, release of a fluorescent probe from synthetic liposomes induced by a virus preparation. Standard virus preparation (IBDV) induces a small leak of the liposomes. When EDTA is added at a 1 mM concentration, the leakage of the fluorescent compound is increased (IBDV+EDTA). When calcium at a concentration of 5 mM is present, the leakage of the fluorescent compound is inhibited. Subviral particles only containing the capsid protein VP2 (SVP/VP2) do not have any effect on liposomes. EDTA does not severely damage the virus as observed by electron microscopy and by the fact that EDTA treated virions recovered partial infectivity in the presence of calcium. *B*, effect of calcium concentration on virus infectivity. Numbers of infected cells, expressed as a percentage of cells infected in a Tris-buffered isotonic solution (NaCl 0.9%), are presented for different calcium concentrations. To efficiently infect a cell culture, the inoculum needs to contain 0.2 mM calcium. Altogether, this figure shows that calcium plays a critical role in infection; it is required for an early step of the infection and needs to be depleted to promote pep46 release from the particles and destabilization of the endosome membrane. *C*, fluorescence-activated cell sorter analysis of the binding of fluorescent virus-like particles (VLP) on permissive (LSCC-BK3) and nonpermissive (DT40) avian lymphoid cell lines. On the *left* and *middle* panels, binding was measured in the presence (red lines) or in the absence (blue lines) of calcium. The *left* panel shows that nonpermissive cells do not allow the binding of VLP independently of the calcium concentration. The *middle* panel shows that permissive cells bind VLP in the presence of calcium. The *right* panel shows that VLP bound to permissive cells in the presence of calcium (red line) are partially released by EDTA treatment (blue lines). The green lines in all panels indicate the fluorescence signal detected on cells that are not incubated with fluorescent VLP.

sufficient to destabilize membranes; however, the activity is increased when a proline, and its isomerization property, is present at position 16. All these observations suggest that pep46 plays a crucial role in cell entry. To be active, pep46 in the virus needs to be accessible to membranes during entry.

*The Activity of pep46 Present in the Virus Particle Is Controlled by the Divalent Ion Concentration*—Using the fluorescent probe release assay, we found that purified viruses induce a weak leakage of the liposomes (see Fig. 5*A*). The release of the probe is greatly increased when calcium is chelated by addition of EDTA and reduced when calcium is added. Subviral particles only constituted by the capsid protein VP2 (particles that do not contain pep46) do not induce liposome leakage. Neither pH variations nor protease treatments are capable of promoting pore formation by the virus particles (not shown). These results demonstrate that the main effector of

the activity of the virus on membranes is the calcium concentration. It is reasonable to assume that the membrane activity of the virus is due to the release of pep46 from the virions. We attribute the membrane activity of purified IBDV preparations to the presence of partially disrupted virions. Interestingly, it was previously demonstrated for rotavirus, another dsRNA virus, that release of the external capsid proteins (VP4 and VP7) that leads to the generation of membrane-active peptides is also controlled by calcium concentration (24). It has been shown that the concentration of calcium in endosomes is as low as 3–30 μM (32, 33), suggesting that the peptide is released in the endosomes. All these observations suggest that birna- and rotaviruses use similar entry pathways.

To further investigate the role of calcium in cell entry, infections were carried out at various calcium concentrations. Fig. 5*B* shows indeed that infection is highly depend-



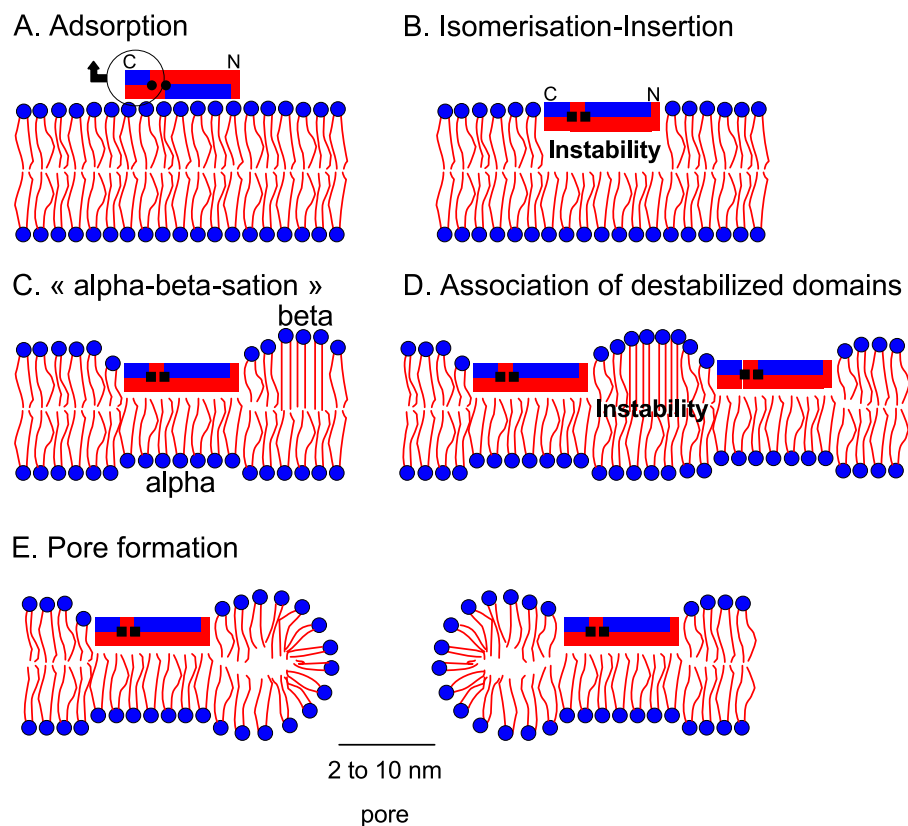


**FIGURE 7. Schematic model for membrane deformation and pore formation induced by a viral amphipathic peptide.** *A*, peptide adsorbed to the lipid polar head surface (colored in blue) by its hydrophilic side (blue), presenting its hydrophobic side (colored in red) to the aqueous solvent. Prolines in the *trans* conformation are indicated by black-filled circles. The lipid aliphatic chains are colored in red. The circle and the kinked arrow indicate the domain that can change orientation with the proline isomerizations when adsorbed to the lipid polar heads. *B*, prolines change conformation from *trans* to *cis* (black squares) and the peptide rotates and inserts its hydrophobic side into the bilayer, excluding lipid molecules. The red star indicates instability in the membrane introduced by the peptide insertion. *C*, bilayer rearranges leading to a thinning of the membrane as observed by microscopy. Peptide insertion results in an ordering of the lipid aliphatic chains; the peptide forces the aliphatic chains of the target leaflet to adopt a  $\beta$ -conformation. To compensate the membrane surface increase resulting from the peptide insertion, the aliphatic chains of the opposite layer are disorganized and adopt an  $\alpha$ -conformation. The peptide “alpha-beta-zes” the membrane. *D*, when several alpha-beta-zed domains become adjacent, instability is created that leads to the formation of a pore (*E*).

the N- and C-terminal domains of pep46. Two of the four positively charged residues of the N-terminal domain (Lys<sup>4</sup> and Arg<sup>11</sup>) cannot be substituted. Conversely, single substitutions of the negatively charged residues of the C-terminal domain allow virus amplification. No virus was recovered with most substitutions of the hydrophobic residues of the N- and C-terminal domains. In the central proline-rich domain, only two residues are critical for virus rescue: Pro<sup>16</sup> and Ala<sup>25</sup>. Most of the substitutions of alanine by arginine are critical to virus rescue, suggesting that such mutations induce important structural destabilization. Interestingly, the substitution of a hydrogen atom by a methyl group (glycine to alanine at position 35) is deleterious for virus rescue, showing that the flexibility between the two last  $\alpha$ -helices is essential for pep46 function.

In conclusion, the reverse genetic experiments indicate that the two terminal domains of pep46 are critical to the viral cycle. Pep46 may be involved in numerous virus functions such as assembly (34), genome packaging. However, as expected for a membrane-interacting peptide, the

amphipathicity of pep46 has to be preserved for virus viability. Pro<sup>16</sup>, the proline belonging to the membrane-active domain of pep46, cannot be substituted, suggesting that the bending induced by this residue between the two first helices, and its isomerization properties are critical to the virus survey. Reverse genetics also shows that the C-terminal domain plays a role in the viral cycle. Because the N terminus of pep46 is sufficient to induce pores in liposomes, the C terminus appears involved in other function such as the association of pep46 to the virions.

*Conclusions: a Model for the Entry of Birnaviruses—*Altogether, these observations suggest that pep46 is involved in a multi-step entry mechanism. In the presence of calcium, the virus recognizes its target cell and is endocytosed. Next, we propose that the low calcium concentration of the endosome allows the release of pep46 from the virus particle and the deformation of the membranes. The final step of the membrane destabilization is the formation of pores. The model shown in Fig. 7 is a tentative explanation of the pore formation process that takes into account the biophysical properties of the peptide and the observed structure of the membranes. The amphipathic nature of the N-terminal domain of pep46 at first permits interactions with the polar heads of the lipids constituting the membrane and exposing hydrophobic residues to the solvent (Fig. 7A). We propose that isomerization of Pro<sup>16</sup> increases the exposed hydrophobicity and leads to a rotation of the peptide at the membrane surface. The peptide inserts into the lipids and segregates the aliphatic chains creating instability (Fig. 7B). The lipid segregation within a leaflet and the resulting aliphatic chain interdigitation between leaflets lead to membrane thickness variation as observed by electron cryomicroscopy (Fig. 7C). The peptide insertion orders the aliphatic chains of the target leaflet while it disorders the ones of the opposite leaflet. In other words, according to the Luzzati nomenclature (35), the peptide insertion has a tendency to favor a  $\beta$  lipid conformation in the insertion leaflet and an  $\alpha$  conformation in the opposite one. In others words, the peptide “alpha-beta-zes” the membrane around its insertion position. We do not know how many peptides are required for the formation of one pore but the existence of a lag time in this process indeed suggests that several peptides are involved.

## A Viral Peptide Deforms and Perforates Membrane

When two or more “alpha-beta-zed” membrane domains come close together (Fig. 7D), the instability of the membrane leads to the formation of a pore (Fig. 7E). The fact that both termini of pep22 are accessible suggests that the peptide remains close to the polar heads of the lipids. The diameter of the pore (less than 10 nm) is smaller than that of the virus (70 nm), suggesting that exchange of small molecules between endosomal ghosts and the cytoplasm is sufficient to allow the initial transcription of the genome and then translation. At this moment, the becoming of the destabilized membrane is not understood. It may stay around the viral particle or be further degraded through physical (osmotic pressure) or biochemical (degradation enzymes) processes.

Finally, this entry model elaborated on a double-stranded RNA virus, a birnavirus, applies to single-strand RNA viruses such as noda- and tetra-viruses (9). All these viruses possess at least one structural peptide of about 40 residues able to destabilize membranes. In agreement with the structural homologies observed for their capsid proteins, single- and double-stranded RNA viruses display almost identical membrane destabilization properties. This observation suggests, as already proposed (15) that single-strand RNA viruses and birnaviruses have a common evolution lineage. Because the replication of double-stranded RNA viruses require the translocation of a large particle through membranes, birnaviruses appeared to have developed high pore formation efficiency by encoding a membrane active peptide containing a proline and its associated *cis-trans* isomerization.

*Acknowledgments*—We thank Yves Gaudin, Jean-Michel Peyrin, Félix Rey, Human Rezaei, and Stéphane Roche for helpful discussions.

### REFERENCES

- Smith, A. E., and Helenius, A. (2004) *Science* **304**, 237–242
- Wilson, I. A., Skehel, J. J., and Wiley, D. C. (1981) *Nature* **289**, 366–373
- Bullough, P. A., Hughson, F. M., Skehel, J. J., and Wiley, D. C. (1994) *Nature* **371**, 37–43
- Roche, S., Bressanelli, S., Rey, F. A., and Gaudin, Y. (2006) *Science* **313**, 187–191
- Heldwein, E. E., Lou, H., Bender, F. C., Cohen, G. H., Eisenberg, R. J., and Harrison, S. C. (2006) *Science* **313**, 217–220
- Hogle, J. M. (2002) *Annu. Rev. Microbiol.* **56**, 677–702
- Bubeck, D., Filman, D. J., and Hogle, J. M. (2005) *Nat. Struct. Mol. Biol.* **12**, 615–618
- Wery, J. P., Reddy, V. S., Hosur, M. V., and Johnson, J. E. (1994) *J. Mol. Biol.* **235**, 565–586
- Bong, D. T., Steinem, C., Janshoff, A., Johnson, J. E., and Reza Ghadiri, M. (1999) *Chem. Biol.* **6**, 473–481
- Janshoff, A., Bong, D. T., Steinem, C., Johnson, J. E., and Ghadiri, M. R. (1999) *Biochemistry* **38**, 5328–5336
- Maia, L. F., Soares, M. R., Valente, A. P., Almeida, F. C., Oliveira, A. C., Gomes, A. M., Freitas, M. S., Schneemann, A., Johnson, J. E., and Silva, J. L. (2006) *J. Biol. Chem.* **238**, 29278–29286
- Chandran, K., and Nibert, M. L. (2003) *Trends Microbiol.* **11**, 374–382
- Agosto, M. A., Ivanovic, T., and Nibert, M. L. (2006) *Proc. Natl. Acad. Sci. U. S. A.* **103**, 16496–16501
- Zhang, L., Chandran, K., Nibert, M. L., and Harrison, S. C. (2006) *J. Virol.* **80**, 12367–12376
- Coulibaly, F., Chevalier, C., Gutsche, I., Pous, J., Navaza, J., Bressanelli, S., Delmas, B., and Rey, F. A. (2005) *Cell* **120**, 761–772
- Saugar, I., Luque, D., Ona, A., Rodriguez, J. F., Carrascosa, J. L., Trus, B. L., and Caston, J. R. (2005) *Structure* **13**, 1007–1017
- Bottcher, B., Kiselev, N. A., Stel'Mashchuk, V. Y., Perevozchikova, N. A., Borisov, A. V., and Crowther, R. A. (1997) *J. Virol.* **71**, 325–330
- Pous, J., Chevalier, C., Ouldali, M., Navaza, J., Delmas, B., and Lepault, J. (2005) *J. Gen. Virol.* **86**, 2339–2346
- Tacken, M. G., Peeters, B. P., Thomas, A. A., Rottier, P. J., and Boot, H. J. (2002) *J. Virol.* **76**, 11301–11311
- Lombardo, E., Maraver, A., Cast n, J. R., Rivera, J., Fernandez-Arias, A., Serrano, A., Carrascosa, J. L., and Rodriguez, J. F. (1999) *J. Virol.* **73**, 6973–6983
- Delmas, B., Kibenge, F. S. B., Leong, J. C., Mundt, E., Vakharia, V. N., and Wu, J. L. (2005) *Birnaviridae*, Academic Press, London
- Da Costa, B., Chevalier, C., Henry, C., Huet, J. C., Petit, S., Lepault, J., Boot, H., and Delmas, B. (2002) *J. Virol.* **76**, 2393–2402
- Birghan, C., Mundt, E., and Gorbalenya, A. E. (2000) *EMBO J.* **19**, 114–123
- Nandi, P., Charpilienne, A., and Cohen, J. (1992) *J. Virol.* **66**, 3363–3367
- Adrian, M., Dubochet, J., Lepault, J., and McDowell, A. W. (1984) *Nature* **308**, 32–36
- Kumar, A., Ernst, R. R., and Wuthrich, K. (1980) *Biochem. Biophys. Res. Commun.* **95**, 1–6
- Piotto, M., Saudek, V., and Sklenar, V. (1992) *J. Biomol. NMR* **2**, 661–665
- Nilges, M., Clore, G. M., and Gronenborn, A. M. (1988) *FEBS Lett.* **239**, 129–136
- Brünger, A. T., Adams, P. D., Clore, J. M., DeLano, W. L., Gros, P., Grosse-Kunstleve, R. W., Jiang, J. S., Kuszewski, J., Nilges, M., and Pannu, N. S. (1998) *Acta. Crystallogr.* **D54**, 905–921
- Laskowski, R. A., Rullmann, J. A., MacArthur, M. W., Kaptein, R., and Thornton, J. M. (1996) *J. Biomol. NMR* **8**, 477–486
- Chevalier, C., Lepault, J., Erk, I., Da Costa, B., and Delmas, B. (2002) *J. Virol.* **76**, 2384–2392
- Gerasimenko, J. V., Tepikin, A. V., Petersen, O. H., and Gerasimenko, O. V. (1998) *Curr. Biol.* **8**, 1335–1338
- Gerasimenko, O. V., and Tepikin, A. V. (2005) *Cell Calcium* **38**, 201–211
- Chevalier, C., Galloux, M., Pous, J., Henry, C., Denis, J., Da Costa, B., Navaza, J., Lepault, J., and Delmas, B. (2005) *J. Virol.* **79**, 12253–12263
- Luzzati, V., Tardieu, A., and Gulik-Krzywicki, T. (1968) *Nature* **217**, 1028–1030

**Infectious Bursal Disease Virus, a Non-enveloped Virus, Possesses a Capsid-associated Peptide That Deforms and Perforates Biological Membranes**  
Marie Galloux, Sonia Libersou, Nelly Morellet, Serge Bouaziz, Bruno Da Costa, Malika Ouldali, Jean Lepault and Bernard Delmas

*J. Biol. Chem.* 2007, 282:20774-20784.

doi: 10.1074/jbc.M701048200 originally published online May 8, 2007

---

Access the most updated version of this article at doi: [10.1074/jbc.M701048200](https://doi.org/10.1074/jbc.M701048200)

Alerts:

- [When this article is cited](#)
- [When a correction for this article is posted](#)

[Click here](#) to choose from all of JBC's e-mail alerts

This article cites 34 references, 13 of which can be accessed free at <http://www.jbc.org/content/282/28/20774.full.html#ref-list-1>